Amino Acids (2011) 40:411–420
DOI 10.1007/s00726-010-0651-y

ORIGINAL ARTICLE

Towards non-peptide ANG II AT1 receptor antagonists based on urocanic acid: rational design, synthesis and biological evaluation

George Agelis · Amalia Resvani · Minos-Timotheos Matsoukas · Theodore Tselios · Konstantinos Kelaidonis · Dimitra Kalavrizioti · Demetrios Vlahakos · John Matsoukas

Received: 19 April 2010 / Accepted: 2 June 2010 / Published online: 6 July 2010

Abstract A series of *o*-, *m*- and *p*-benzyl tetrazole derivatives **11a–c** has been designed, synthesized and evaluated as potential Angiotensin II AT1 receptor antagonists, based on urocanic acid. Compound **11b** with tetrazole moiety at the *m*-position showed moderate, however, higher activity compared to the *o*- and *p*-counterpart analogues. Molecular modelling techniques were performed in order to extract their putative bioactive conformations and explore their binding modes.

Keywords AT1 receptor · Urocanic acid · Pharmacophore · Molecular modelling

Introduction

Renin–angiotensin System (RAS) is a well-known cascade playing a pivotal role in cardiovascular homeostasis and its inactivation by an ACE inhibitor (Wyvratt and Patchett 1985) (Captopril, Enalapril etc.), a non-peptide ANG II AT1 receptor blocker (Carini et al. 1991) (Losartan, Irbesartan, Candesartan etc.) or a renin inhibitor (Aliskiren) (Lam and Choy 2007), has been established as a successful therapeutic approach for the treatment of hypertension and other cardiovascular diseases (Dzau 1994). Experimental evidence for ANG II, the primary effector component of RAS, has supported a bioactive conformation characterized by a charge relay system between Tyr hydroxyl, His imidazole and Phe carboxylate (Matsoukas et al. 1994), as well as spatial proximity of the three key amino acids Tyr-His-Phe which seems to be responsible for agonistic activity (Matsoukas et al. 2000; Turner et al. 1990). Thus, conformational analysis using 2 D NMR techniques in receptor-simulating environments has shown proximity of the three key amino acid side chains and the formation of tyrosinate anion has been demonstrated by nanosecond time-resolved fluorescence studies (Turner et al. 1991; Matsoukas et al. 1995).

The DuPont group was the first to develop Losartan (DuP 753) (Chiu et al. 1990), an orally effective ANG II receptor blocker, which is metabolized in vivo to the more potent full antagonist EXP3174 (Wong et al. 1990). Structure–activity relationships (SAR) studies have illustrated the importance of the tetrazole and phenyl groups of Losartan (Carini et al. 1991; Duncia et al. 1990) for binding to the AT1 receptor. Alkyl lipophilic substituents, such as biphenyl group at the 1-position and a linear alkyl group at the 2-position of the imidazole ring gave rise to compounds of higher affinity due to a tight fit into the hydrophobic pocket. On the other hand, remarkable binding affinity emerges in the presence of acidic groups such as carboxyl or its isoster tetrazole group which interacts with the positive charge of the receptor binding site. Furthermore, a

Electronic supplementary material The online version of this article (doi:10.1007/s00726-010-0651-y) contains supplementary material, which is available to authorized users.

G. Agelis (✉) · A. Resvani · M.-T. Matsoukas · T. Tselios · K. Kelaidonis · J. Matsoukas (✉)
Department of Chemistry, University of Patras, 26500 Patras, Greece
e-mail: aggelisgeorge@hotmail.com

J. Matsoukas
e-mail: imats@chemistry.upatras.gr

D. Kalavrizioti
Department of Pharmacology, School of Medicine, University of Patras, 26500 Patras, Greece

D. Vlahakos
Department of Internal Medicine, 'ATTIKON' University Hospital, Athens, Greece

nitrogen atom at the 3-position enhances the activity through hydrogen bonding to the receptor (Thomas et al. 1992).

On the basis of these findings, we designed, synthesized and evaluated a series of benzyl tetrazole compounds **11a–c** based on urocanic acid as potential ANG II receptor antagonists. The reason we used urocanic acid as a template was to replace the imidazole butyl group with an ester group similar to the one in Olmesartan (Yanagisawa et al. 1996) in which the aliphatic moiety is the bulky ester group (5-methyl-2-oxo-1,2-dioxol-4-yl)methyl which in vivo is metabolized to the carboxyl moiety. In particular, replacement of the butyl group of Losartan with propanoic methyl ester may enhance the affinity and act as a prodrug (Kubo et al. 1993). The biphenyl tetrazole functionality of Losartan was replaced by the phenyl tetrazole group, positioning tetrazole moiety at the *o*-, *m*- and *p*-position. The reason for the shortening of the biphenyl group was to evaluate the ability of tetrazole group to trigger activity located on a phenyl group instead of a biphenyl moiety and on the other hand the ability of a single phenyl group to interact with the receptor.

Molecular modelling techniques were applied in order to extract the possible bioactive conformations of the designed compounds. The putative energy minimum conformations of analogues **11a–c** (Fig. 1) were superimposed with the proposed bioactive conformation of EXP3174 (Fig. 5) in order to gain information on the orientation of their pharmacophore groups and were docked to the AT1 receptor, to understand their binding properties. The synthesis of the target compounds **11a–c** included a facile few-step method in high yields. In vitro and in vivo experiments were performed in order to evaluate the antihypertensive activity of these synthesized analogues. Compound **11b** with benzyl tetrazole moiety at the *m*-position showed moderate, however, higher activity compared to the *o*- and *p*-counterpart analogues (Fig. 4).

Materials and methods

General remarks

Starting materials were purchased by Aldrich and used as received. Melting points were determined with a Stuart SMP 10 apparatus and are uncorrected. ^{1}H NMR and ^{13}C NMR spectra were recorded on a Bruker Avance DPX spectrometer at 400.13 and 100.62 MHz, respectively. Chemical shifts are reported in units, parts per million (ppm) downfield from tetramethylsilane (TMS) and coupling constants (*J*) are given in Hertz (Hz). HPLC analysis was performed on a Alliance Waters 2695 equipped with a Waters 2996 Photodiode Array Detector UV–vis, using a XBridge C18 column (4.6 × 150 mm, 3.5 μm). Electrospray ionization mass spectra (ESI–MS) were obtained on a Electrospray Platform LC instrument HRMS experiments were carried out in a micrOTOF-II (University of Notre Dame, Indianapolis, USA) mass spectrometer equipped with an ion spray ionization source. Microanalyses were performed on a Carlo Erba EA 1108 CHNS elemental analyser in the Laboratory of Instrumental Analysis of the University of Patras. All reactions were carried out in dry solvents. TLC was performed on silica gel 60 F_{254} plates (Merck, Germany). Purification of final products was performed with Waters Preparative HPLC (Waters Prep LC Controller) using SunFire Prep C_{18} column (50 × 100 mm) with 5 μm packing material. Separation was performed with stepped linear gradient from 5% acetonitrile to 90% acetonitrile in 50 min with a flow rate of 9 mL/min. Supplementary data are also available.

General synthesis of alkyl bromides **5a–c**

A solution of **1a** (7.8 mL, 66.24 mmol), NaN_3 (4.31 g 66.24 mmol), Sn(*n*-Bu)$_3$Cl (19.76 mL, 72.86 mmol) in dry Tol (35 mL) was refluxed for 4 days. After completion of the reaction, the solvent was evaporated resulting in a colourless oil **2a** used in the next reaction without further purification. Compound **2a** (20.86 g, 46.37 mmol) was dissolved in a mixture of THF (60 mL), H_2O (20 mL), 2 N HCl (26 mL, 52 mmol) and stirred at RT. After 16 h, the solvents were concentrated and the residue was diluted in H_2O (80 mL), extracted with EtOAc (3 × 100 mL) and the organic layer was washed with Brine, dried and concentrated. The oily residue **3a** (0.77 g, 44.05 mmol) was dissolved in DCM (110 mL), TEA (15.50 mL, 110.12 mmol), TrtCl (13.47 g, 48.45 mmol) were added and stirred at RT for 1 h. The mixture was diluted with DCM, washed successively with 5% w/v $NaHCO_3$ (×3), H_2O (×2), dried over Na_2SO_4 and concentrated. Recrystallization from diisopropyl ether (DIE) afforded **4a** as a white solid. A mixture of **4a** (14.80 g, 37.0 mmol), NBS (6.58 g, 37.0 mmol), DBP (0.89 g, 3.7 mmol) in CCl_4 (100 mL) was refluxed for 8 h. The mixture was allowed to cool at 40°C, the yellow solid was filtered off and the filtrate was concentrated in vacuo. The oily residue was recrystallized from DIE to afford **5a** as a pure white solid (13.85 g, 78%). Compounds **5b–c** were prepared by a similar procedure.

Data for compound **4a**: Yield: 84%; mp 140–142°C; ESI–MS (*m/z*): 160.37 (M + H$^+$-Trt), 243.23 (Trt); ^{1}H NMR (400 MHz, $CDCl_3$): δ (ppm) 8.05 (d, 1H, J = 7.1 Hz), 7.33–7.14 (m, 18H), 2.48 (s, 3H); ^{13}C NMR (100 MHz, $CDCl_3$): δ (ppm) 164.13, 140.71, 139.24, 137.58, 136.33, 131.88, 129.91, 129.50, 128.40, 127.96, 125.59, 126.52, 125.94, 81.98, 21.74; Anal. Calcd for $C_{27}H_{22}N_4$: C, 80.57, H, 5.51, N, 13.92. Found: C, 80.66, H, 5.63, N, 14.05.

Data for compound **4b**: Yield: 85%; mp 139–141°C; ESI–MS (*m/z*): 160.33 (M + H$^+$-Trt), 242.85 (Trt); ^{1}H NMR (400 MHz, $CDCl_3$): δ (ppm) 7.97–7.93 (m, 2H),

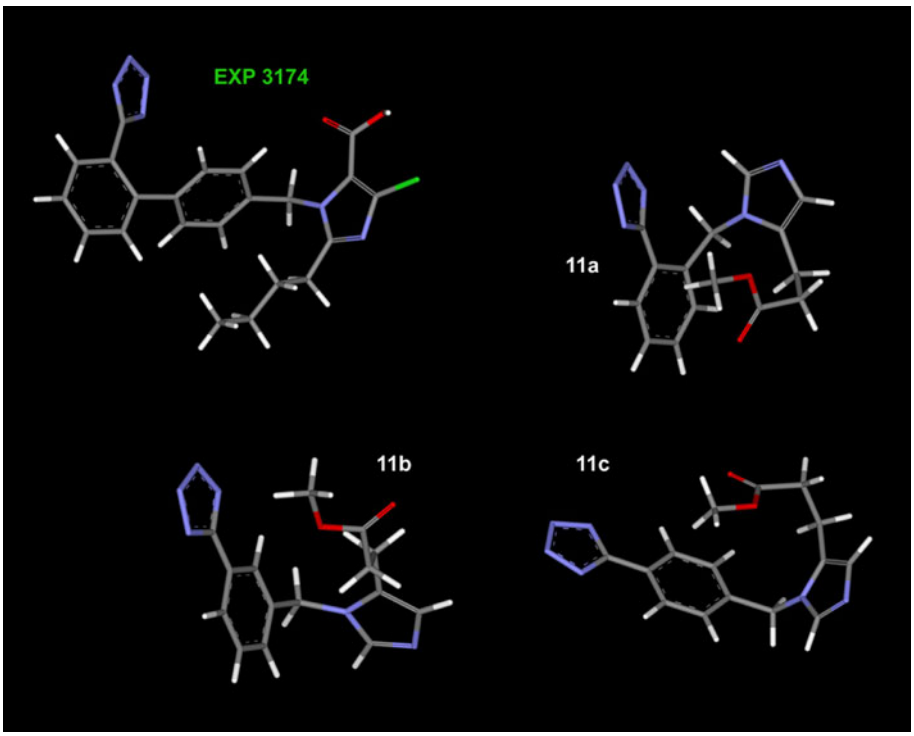

Fig. 1 Energy minima of **EXP3174** and compounds **11a–c** after molecular modelling simulations which consisted of Energy Minimization, Molecular Dynamics and Energy Minimization runs sequentially for a total time of 1 ns

7.37–7.16 (m, 17H), 2.41 (s, 3H); ^{13}C NMR (100 MHz, $CDCl_3$): δ (ppm) 164.55, 141.79, 138.91, 131.40, 130.68, 129.78, 129.48, 129.06, 128.68, 128.39, 128.15, 127.96, 127.79, 127.63, 127.17, 124.59, 83.44, 21.73; Anal. Calcd for $C_{27}H_{22}N_4$: C, 80.57, H, 5.51, N, 13.92. Found: C, 80.43, H, 5.41, N, 13.78.

Data for compound **4c**: Yield: 87%; mp 146–148°C; ESI–MS (*m/z*): 160.34 ($M + H^+$-Trt), 242.75 (Trt); ^{1}H NMR (400 MHz, $CDCl_3$) δ (ppm) 8.03 (d, 2H, $J = 8.0$ Hz), 7.35–7.16 (m, 17H), 2.40 (s, 3H); ^{13}C NMR (100 MHz, $CDCl_3$): δ (ppm) 164.14, 141.45, 140.42, 130.34, 129.48, 128.32, 127.95, 127.78, 127.33, 127.00, 124.76, 83.04, 21.53; Anal. Calcd for $C_{27}H_{22}N_4$: C, 80.57, H, 5.51, N, 13.92. Found: C, 80.72, H, 5.69, N, 13.82.

Data for compound **5a**: Yield: 78%; mp 135–137°C; ESI–MS (*m/z*): 239.17 ($M + H^+$-Trt), 243.23 (Trt); HRMS-ESI (*m/z*): $[M + Na]^+$ calcd for $C_{27}H_{21}BrN_4Na$, 503.0847; found, 503.0835; ^{1}H NMR (400 MHz, $CDCl_3$): δ (ppm) 8.19–8.17 (m, 1H), 7.49–7.19 (m, 18H), 4.92 (s, 2H); ^{13}C NMR (100 MHz, $CDCl_3$): δ (ppm) 162.90, 141.28, 136.74, 131.54, 130.44, 130.36, 130.15, 128.94, 128.41, 127.94, 127.85, 127.29, 126.34, 83.44, 32.42; Anal. Calcd for $C_{27}H_{21}BrN_4$: C, 67.37, H, 4.40, N, 11.64. Found: C, 67.58, H, 4.56, N, 11.78.

Data for compound **5b**: Yield: 79%; mp 137–139°C; ESI–MS (*m/z*): 239.07 ($M + H^+$-Trt), 243.16 (Trt); HRMS-ESI (*m/z*): $[M + Na]^+$ calcd for $C_{27}H_{21}BrN_4Na$, 503.0847; found, 503.0833; ^{1}H NMR (400 MHz, $CDCl_3$): δ (ppm) 8.10–8.08 (m, 1H), 7.50–7.16 (m, 18H), 4.54 (s, 2H); ^{13}C NMR (100 MHz, $CDCl_3$): δ (ppm) 163.91, 141.65, 139.94, 131.35, 130.66, 129.78, 128.77, 128.44, 128.30, 128.21, 128.17, 127.83, 127.64, 127.47, 124.78, 83.66, 33.19; Anal. Calcd for $C_{27}H_{21}BrN_4$: C, 67.37, H, 4.40, N, 11.64. Found: C, 67.43, H, 4.31, N, 11.54.

Data for compound **5c**: Yield: 78%; mp 136–138°C; ESI–MS (*m/z*): 239.17 ($M + H^+$-Trt), 243.10 (Trt); HRMS-ESI (*m/z*): $[M + Na]^+$ calcd for $C_{27}H_{21}BrN_4Na$, 503.0847; found, 503.08336; ^{1}H NMR (400 MHz, $CDCl_3$): δ (ppm) 8.13 (d, 2H, $J = 8.3$ Hz) 7.49–7.16 (m, 17H), 4.52 (s, 2H); ^{13}C NMR (100 MHz, $CDCl_3$): δ (ppm) 163.53, 146.86, 141.32, 139.88, 132.45, 130.31, 130.09, 129.51, 129.30, 128.39, 127.94, 127.82, 127.50, 127.34, 127.28, 127.10, 83.26, 32.85; Anal. Calcd for $C_{27}H_{21}BrN_4$: C, 67.37, H, 4.40, N, 11.64. Found: C, 67.28, H, 4.62, N, 11.49.

Methyl urocanate **7**

A mixture of urocanic acid **6** (1 g, 7.24 mmol), anhydrous Na_2SO_4 (0.14 g, 1 mmol) and conc. H_2SO_4 (1 mL) in dry MeOH (15 mL) was refluxed for 24 h. After completion of the reaction the solid Na_2SO_4 was filtered off, the solvent was removed in vacuo and the residue was diluted in EtOAc, washed successively with saturated $NaHCO_3/H_2O$ (×3) and Brine (×1), dried and concentrated. Precipitation with petroleum ether (40–70°C) afforded pure **7** as a white solid (0.99 g, 90%).

Data for compound **7**: mp 92–94°C; ESI–MS (*m/z*): 153.22 ($M + H^+$); ^{1}H NMR (400 MHz; CD_3OD): δ (ppm) 7.78 (s, 1H), 7.61 (d, 1H, $J = 16.0$ Hz), 7.43 (s, 1H), 6.44 (d, 1H, $J = 16.0$ Hz), 4.85 (s, 3H); ^{13}C NMR (100 MHz,

CD_3OD): δ (ppm) 168.14, 137.43, 135.25, 134.35, 124.0, 114.35, 50.61. All data were consistent with literature (Pirrung and Pei 2000).

Methyl 3-(imidazol-4-yl)propionate **8**

A solution of **7** (1 g, 6.58 mmol) in MeOH (10 mL) was introduced in a hydrogenation flask and 0.10 g of Pd–C (10%) was added as catalyst. The mixture was stirred under H_2 for 8 h at RT and after completion of the reaction, the catalyst was filtered through a pad of Celite and the filtrate was concentrated in vacuo to furnish a white solid **8** (0.96 g, 95%) which showed adequate purity for the next step.

Data for compound **8**: mp 95–97°C; ESI–MS (*m/z*): 155.41 ($M + H^+$); ^1H NMR (400 MHz, CD_3OD): δ (ppm) 7.58 (s, 1H), 6.81 (s, 1H), 3.66 (s, 3H), 2.88 (t, 2H, $J = 7.2$ Hz), 2.66 (t, 2H, $J = 7.2$ Hz); ^{13}C NMR (100 MHz, CD_3OD): δ (ppm) 173.59, 135.96, 134.53, 115.75, 50.67, 33.27, 21.76. All data were consistent with literature (Pirrung and Pei 2000).

Methyl 3-(1-tritylimidazol-4-yl)propionate **9**

To a solution of compound **8** (1.0 g, 6.53 mmol) in DCM (7 mL) were added TEA (1.80 mL, 13.06 mmol), TrtCl (2.0 g, 7.18 mmol) and the resulting solution was stirred at RT for 2 h. The mixture was diluted with DCM, washed successively with 5% w/v $NaHCO_3$ (×3), H_2O (×2), dried over Na_2SO_4 and concentrated. Recrystallization from DIE afforded **9** (2.25 g, 87%) as a white solid.

Data for compound **9**: mp 142–143°C; ESI–MS (*m/z*): 397.33 ($M + H^+$); ^1H NMR (400 MHz, $CDCl_3$): δ (ppm) 8.02 (s, 1H), 7.42–7.08 (m, 15H), 6.75 (s, 1H), 3.62 (s, 3H), 3.07 (t, 2H, $J = 7.2$ Hz), 2.85 (t, 2H, $J = 7.2$ Hz); ^{13}C NMR (100 MHz, $CDCl_3$): δ (ppm) 173.05, 141.10, 136.45, 129.94, 129.16, 128.86, 128.86, 128.29, 84.33, 51.97, 33.42, 22.06. All data of compounds were consistent with literature (Pirrung and Pei 2000).

General synthesis of alkylated compounds **11a–c**

To a solution of **9** (1.0 g, 2.53 mmol) in dry DCM (7 mL), alkyl bromide **5a** (1.46 g, 3.04 mmol) was added under N_2 atmosphere and the reaction was allowed to proceed for 48 h at RT. The mixture was concentrated *in vacuo* and trituration with DEE afforded **10a** as a yellow solid (1.32 g, 60%), used as obtained for the next step. A solution of **10a** (1.0 g, 1.14 mmol) in 2 mL TFA/DCM (1:1) in the presence of TES (0.15 mL, 1 mmol) was stirred at RT and after 1 h the solvent was concentrated. Trituration with DEE afforded a yellow solid, followed by purification with preparative RP-HPLC (5% acetonitrile to 90% acetonitrile in 50 min with a flow rate of 9 mL/min) and lyophilization furnished pure **11a** as a white foam (0.49 g, 80%). Compounds **11b–c** were prepared by a similar procedure.

Data for compound **11a**: ESI–MS (*m/z*): 313.30 ($M + H^+$); HRMS-ESI (*m/z*): $[M + H]^+$ calcd for $C_{15}H_{17}N_6O_2$, 313.1413; found, 313.1401; ^1H NMR (400 MHz, CD_3OD): δ 8.54 (s, 1H), 7.99–7.97 (m, 1H), 7.66–7.61 (m, 2H), 7.40–7.38 (m, 1H), 7.35 (s, 1H), 5.80 (s, 2H), 3.65 (s, 3H), 2.93 (t, 2H, $J = 7.2$ Hz), 2.69 (t, 2H, $J = 7.2$ Hz); ^{13}C NMR (100 MHz, CD_3OD): δ (ppm) 172.72, 157.78, 135.35, 134.87, 132.17, 131.30, 130.54, 130.26, 129.97, 126.19, 117.24, 51.37, 49.24, 31.26, 18.88; Anal. Calcd for $C_{17}H_{17}F_3N_6O_4$: C, 47.89, H, 4.02, N, 19.71. Found: C, 47.96, H, 4.11, N, 19.62.

Data for compound **11b**: ESI–MS (*m/z*): 313.30 ($M + H^+$); HRMS-ESI (*m/z*): $[M + H]^+$ calcd for $C_{15}H_{17}N_6O_2$, 313.1413; found, 313.1403; ^1H NMR (400 MHz, CD_3OD): δ (ppm) 8.99 (s, 1H), 8.04 (d, 1H, $J = 7.8$ Hz), 7.94 (s, 1H), 7.64 (t, 1H, $J = 7.8$ Hz), 7.50 (d, 1H, $J = 7.8$ Hz), 7.42 (s, 1H), 5.60 (s, 2H), 3.60 (s, 3H), 2.93 (t, 2H, $J = 7.2$ Hz), 2.64 (t, 2H, $J = 7.2$ Hz); ^{13}C NMR (100 MHz, CD_3OD): δ (ppm) 172.70, 157.65, 135.90, 135.60, 134.65, 130.44, 129.98, 127.46, 127.13, 126.09, 117.95, 51.34, 49.88, 31.32, 18.84; Anal. Calcd for $C_{17}H_{17}F_3N_6O_4$: C, 47.89, H, 4.02, N, 19.71. Found: C, 47.81, H, 4.19, N, 19.57.

Data for compound **11c**: ESI–MS (*m/z*): 313.45 ($M + H^+$); HRMS-ESI (*m/z*): $[M + H]^+$ calcd for $C_{15}H_{17}N_6O_2$, 313.1413; found, 313.1406; ^1H NMR (400 MHz, CD_3OD): δ (ppm) 8.98 (s, 1H), 8.09 (d, 2H, $J = 8.2$ Hz), 7.48 (d, 2H, $J = 8.2$ Hz), 7.42 (s, 1H), 5.59 (s, 2H), 3.63 (s, 3H), 2.91 (t, 2H, $J = 7.2$ Hz), 2.66 (t, 2H, $J = 7.2$ Hz); ^{13}C NMR (100 MHz, CD_3OD): δ (ppm) 172.32, 157.67, 136.68, 135.49, 134.27,128.17, 127.62, 125.72, 117.47, 50.97, 49.42, 30.86, 18.42; Anal. Calcd for $C_{17}H_{17}F_3N_6O_4$: C, 47.89, H, 4.02, N, 19.71. Found: C, 47.92, H, 3.95, N, 19.86.

Molecular modelling

Molecular dynamics and minimization

All computer calculations were performed on a Pentium IV workstation equipped with a 2.14 GHz processor using Discovery Studio version 2.0 molecular modelling systems by Accelrys Software Inc. (San Diego, CA, USA). The molecular modelling procedure included Energy Minimization (using the algorithms Steepest Descents for 9000 iterations and Conjugate Gradient for 9000 iterations) using the CHARMm force field. Dielectric constant was set to 45 for better simulation of the receptor environment during all the experiments as well as the SHAKE algorithm and RMSD 0.001 Å as energy convergence criterion. MD runs of EXP3174 and analogues **11a–c**, were performed using the CHARMm force field as follows: Heating, from 0–300 K gradually, and Equilibration were set with a time

step of 0.002 ps for a total time of 0.1 ns while the time step of Production was 0.002 ps for a total time of 1 ns. Parameters on saving results frequencies were set in such a way in order to extract 300 conformations for each molecule. Energy Minimization runs were performed (using the algorithms Steepest Descents for 9000 iterations and Conjugate Gradient for 9000 iterations) on the final 300 conformations, respectively. Analogues **11a–c** were superimposed with the proposed bioactive conformation of EXP3174 in order to compare the groups of our compounds. The conformations of the two rings (imidazole and phenyl) of the studied compounds and EXP3174 were used in the superimpositions in order to determine the orientation of the tetrazole group, which is critical for the antagonistic activity.

Docking studies

The molecular docking techniques provide useful information of drug affinity for the receptor, and various models and studies have been performed on the AT1 receptor and non-peptide antagonists (Tuccinardi et al. 2006; Patny et al. 2006). Our study includes the binding modes of compounds **11a–c** as ANG II antagonists and EXP3174. The AT1 receptor model was generated using the recent human beta-2 adrenergic receptor crystal structure determined at 2.4 Å (2RH1) (Cherezov et al. 2007) as the template. Alignment was performed manually taking into account the highly conserved amino acid residues (Mirzadegan et al. 2003) N1.50, the LA-AD (L2.46, A2.47, A2.49, and D2.50), DRY (D3.49, R3.50 and Y3.51) motif, the tryptophan in the fourth transmembrane helix W4.50, the two prolines P4.59 and P6.50, and the NP–Y motif in TM7 (N7.49, P7.50 and Y7.53). The construction of the receptor was performed by means of the Modeller programme taking into consideration the two disulfide bonds between C18 and C274 as well as between C101 and C180 formed in the extracellular domain. Using the Modeller loop refinement tool, the loops were refined according to the DOPE SCORE (discrete optimized protein energy) assess method, and the receptor was subjected to a molecular dynamics simulation for a time of 2 ns in a vacuum environment, with the backbone of the seven transmembrane helices harmonically restrained in order to allow them some freedom near a particular position in space.

All docking experiments were performed using the CHARMm force field in terms of the Ligandfit method which docks ligands into the active site using a shape filter and Monte-Carlo ligand conformation generation. The important amino acids A3.28(104), N3.35(111), L3.36 (112), Y3.37(113), K5.42(199), W6.48(253), H6.51(256), T6.55(260), A7.42(291), N7.45(294), N7.46(295), C7.47 (296), and L7.48(297), known to effect binding affinity from previous mutagenesis studies (Clement et al. 2005), were located in the binding site of our model. EXP3174 was manually docked in the binding pocket which consists of these residues as the input control ligand in order to define the interaction area. A Monte-Carlo conformation generation was performed for the **11a–c** and EXP3174 compounds in order to obtain a set of various conformations to be docked into the defined binding site. In that stage, the ligands were energy minimized in terms of the Smart Minimizer method, which begins with the Steepest Descent method, followed by the Conjugate Gradient method for faster convergence towards a local minimum in the presence of a fixed or partially flexible receptor. Finally, various scoring functions (PLP1, PLP2, Jain, and PMF) were applied to the ligand–receptor interactions recorded. According to the calculated scores, the best docked poses of each compound were analysed for interaction with the receptor in order to give a detailed explanation of the experimental results.

Biological activity

In vitro studies

Radioligand binding assay We used membrane suspensions containing cloned human ANG II receptor subtype 1 in sf9 cells (AT1 receptor, Perkin Elmer 6110121). In a final volume of 170, 100 µL membrane suspensions (40 µg/µL) were incubated for 120 min at 37°C under mild stirring in assay buffer (20 mM Tris–HCl pH 7.4, 5 mM $MgCl_2$, 1 mM EDTA, 0.1% BSA). The AT1 receptor concentration ($B_{max} = 2.9$ pmol/mg protein) and the affinity of radioligand ($K_d = 0.74$ nM) are available from the manufacturer. In the displacement experiments, the membranes were incubated with 0.5 nM [^{125}I]-Sar^1-Ile^8-ANG II (specific activity 1846 µCi/µg) and investigating ligands at final concentration of 10^{-5} M. Unlabelled ANG II at a concentration of 10 µM was used to estimate non-specific binding. The bound fraction was separated from the free radioligand by rapid vacuum filtration through Millipore GF/C filters. The filters were washed immediately nine times with 500 µL of ice-cold 50 mM Tris–HCl pH 7.4 and the retained radioactivity was measured in gamma counter (Packard Ria Star 5405). Preincubation of GF/C filters with 0.3% polyethylinimine was used to minimize non-specific absorption of the radioligand to filters. All determinations were performed at least three times. Non-specific binding was defined as the amount of radioligand bound in the presence of cold ANG II and specific binding was defined as the total radioligand bound minus non-specific binding.

Intracellular Ca^{2+} ($[Ca^{2+}]_i$) mobilization assay Primary rat aortic smooth muscle cells (RASMCs) were cultured in Dulbecco's modified Eagle's medium (DMEM)

supplemented with 1 mM L-glutamine, 20 mM $NaHCO_3$, 1% streptomycin–penicillin and 10% foetal bovine serum (FBS). Confluent RASMCs were collected by trypsinization (0.05% trypsin, 0.02% EDTA). The cells were washed in loading buffer (145 mM NaCl, 5 mM KCl, 1 mM $MgCl_2$, 1 mM $CaCl_2$, 5.6 mM glucose, 5 mM HEPES, pH 7.4) and then were resuspended in loading buffer plus 0.1% BSA to a final concentration of 4×10^5 cells/mL. Cell suspensions were then incubated with 2.5 μM Fura-2/AM in DMSO for 30 min at 37°C in the dark. After incubation cells were washed extensively with loading buffer, were adjusted to a concentration of 1.5×10^5 cells/mL and were stored at 37°C for 30 min or at RT for 60 min in order hydrolysis of intracellular Fura-2/AM took place. ANG II 10^{-6} μ was added directly to promote Ca^{2+} mobilization. RASMCs were pretreated with the test substances at a concentration of 10^{-5} M for 300 s. Calcium transients were measured with a PERKIN ELMER LS45 spectrofluorometer at RT to minimize compartmentalization and cell extrusion of the fluorescent dye (excitation at 340 and 380 nm, emission at 505 nm). The level of Ca^{2+} mobilization was determined from the excitation ratio of 340 and 380 nm ($R = F_{340}/F_{380}$).

In vivo studies

Adult normotensive male New Zealand white rabbits, weighing between 2.5 and 3.3 kg, were anaesthetized by pentobarbitone (30 mg/kg) via an ear vein, intubated and mechanically ventilated with 100% oxygen using a respirator for small animals. The tidal volume was 15 mL and the rate was adjusted to keep blood gases within normal range. ANG II dependent hypertension was induced by infusing ANG II via a syringe pump through a pre-inserted polyethylene catheter at a constant rate of 0.2 mL/min (1 μg/min). After the establishment of hypertension, three boluses of each compound **11a–c** of 0.5, 1 and 2 mg were administrated via the jugular vein and the changes of blood pressure were recorded through a transducer attached to a multichannel recorder. ANG II and test antagonist were diluted in 5% dextrose.

Results and discussion

Chemistry

The synthetic procedure for titled compounds **11a–c** was divided in two steps. The first step (Fig. 2) involved the synthesis of the *o*-, *m*- and *p*-bromomethylphenyltetrazoles **5a–c** by conversion of the tolunitriles **1a–c** to the corresponding organostannanes **2a–c** with tributyltin choride ($Sn(n\text{-}Bu)_3Cl$) and sodium azide (NaN_3) in 70% yield (Luitjen et al. 1963; Sisido et al. 1971). Acid hydrolysis with 2 N HCl in H_2O/THF (1:3), followed by tritylation of tetrazole using trityl chloride (TrtCl) furnished 1*H*-tetrazole derivatives **4a–c** in high yield (85%). Bromo-derivatives **5a–c** were prepared by bromination with (*N*-bromosuccinimide) NBS and dibenzoyl peroxide (DBP) as initiator in 78% yield. The ^{1}H NMR spectra of **5a–c** were similar, showing singlet peaks at δ 4.92, 4.54, 4.52, respectively, due to the methylene protons, whereas the phenyl protons were observed at the aromatic region as multiplet peaks.

The second step included esterification, reduction, tritylation and selective N^{π} alkylation of urocanic acid (Fig. 3). Thus, urocanic methyl ester **7** resulted from esterification with dry MeOH in the presence of concentrated H_2SO_4 and Na_2SO_4 in 90% yield (Pirrung and Pei 2000). ^{1}H NMR data of **7** showed two singlet peaks at δ 7.78 and 7.43 corresponding to the H-2 and H-5 of the imidazole ring. Moreover, the two vinylic protons appeared as doublets at δ 6.44 and 7.61 ($J = 16.0$ Hz), respectively, while methyl protons were located at δ 4.85 as a singlet peak. The resulting ester was subjected to hydrogenation in the presence of catalyst 10% Pd–C in MeOH to afford **8** in 95% yield. The ^{1}H NMR spectra of **8** showed two triplet peaks at δ 2.88 and 2.66 ($J = 7.2$ Hz), assigned to the methylene protons.

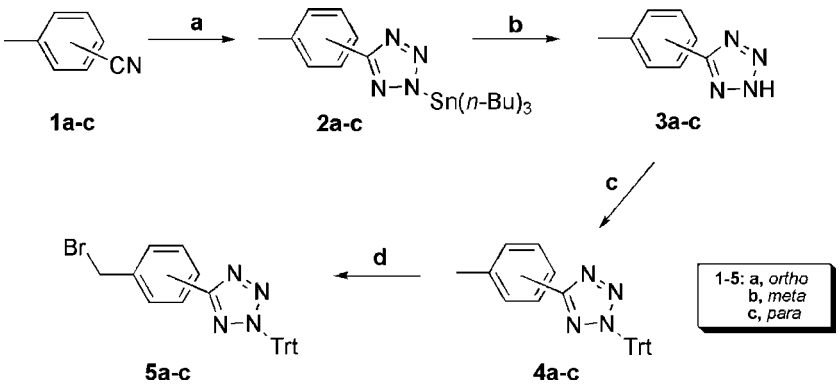

Fig. 2 Reagents and conditions. **a** $Sn(n\text{-}Bu)_3Cl$, NaN_3, Tol, 110°C, 96 h; **b** 2 N HCl in THF/H_2O (3:1), RT, 16 h; **c** TrtCl, TEA, DCM, RT, 1 h; **d** NBS, 10% DBP, CCl_4, reflux, 8 h

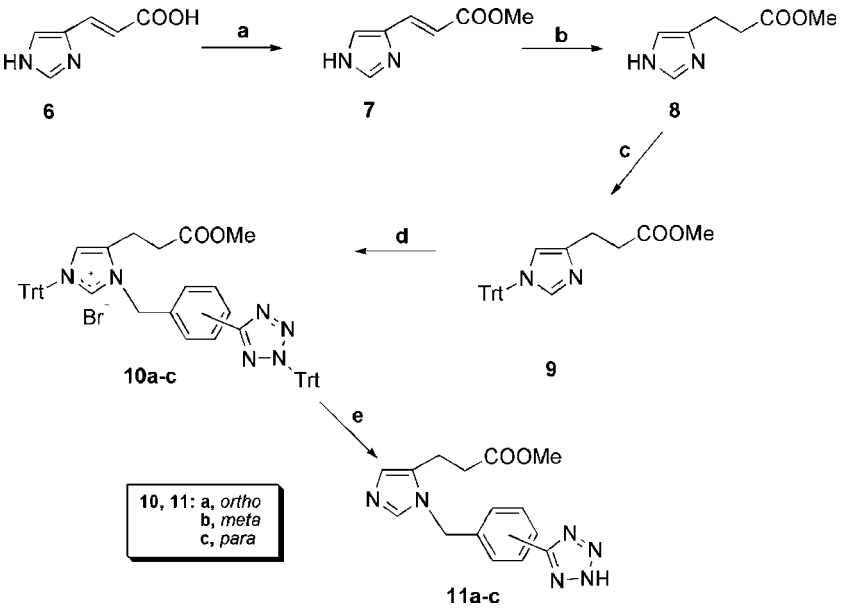

Fig. 3 Reagents and conditions. **a** MeOH, conc. H_2SO_4, Na_2SO_4, reflux, 24 h; **b** H_2, 10% Pd–C, MeOH, RT, 24 h; **c** TrtCl, TEA, DCM, RT, 1 h; **d** 5a–c, DCM, RT, 48 h; **e** TFA/DCM (1:1), TES, RT, 1 h

Protection of the N^{τ}-position was achieved by the sterically demanding trityl blocking group. Thus, tritylation of **8** with TrtCl and triethylamine (TEA) in DCM afforded only the N^{τ}**-** substituted analogue **9** in 87% yield. The ^{1}H NMR spectra showed two singlet peaks at δ 8.02 and 6.75 corresponding to the H-2 and H-5 of the imidazole ring and a multiplet peak at δ 7.42–7.08 due to the 15 phenyl protons. Selective N^{π} alkylation of **9** with **5a–c** in dry DCM for 2 days afforded the fully protected **10a–c** in 60% yield (Lauth-de Viguerie et al. 1994). Moderate yield was owed to the tendency of the trityl group to be eliminated during the alkylation, giving a mixture of N^{π}-substituted and N^{τ}, N^{π}-disubstituted products (Lauth-de Viguerie et al. 1994; Anthony et al. 1999). Deprotection of the Trt group with trifluoroacetic acid (TFA)/DCM (1:1) in the presence of triethylsilane (TES) as scavenger provided the final target compounds **11a–c** after purification in 80% yield as TFA salts. The ^{1}H NMR spectra of **11a–c** showed singlet peaks at δ 5.80, 5.60, 5.59, respectively, due to the methylene protons of the alkylating moiety. Purification of **11a–c** was performed by preparative RP-HPLC using C_{18} column as stationary phase and identification by ESI–MS, ^{1}H NMR and ^{13}C MNR.

Biological activity

The new synthesized compounds **11a–c** were initially evaluated in radioligand binding and intracellular Ca^{2+} mobilization assay (in vitro) at a final concentration of 10^{-5} μ. Although the used concentration was high enough, there were indications for mild to moderate activity of substance **11b** which required further study. Competitive binding experiments revealed that **11b** caused 25% displacement of [^{125}I]-Sar^1-Ile^8-ANG II from the AT1 receptors, whereas Losartan at the same conditions caused 100% displacement. In case of intracellular Ca^{2+} mobilization assay, the stimulation of AT1 receptors with ANG II in concentrations of 10^{-6} M causes the mobilization of intracellular Ca^{2+} from endoplasmic reticulum to cytoplasm and is detected using dye Fura-2/AM. The test substance **11b** was found to induce a 37% inhibition of the ANG II action in contrast with the reference AT1 antagonist Losartan which caused a complete inhibition.

Moreover, compounds **11a–c** were evaluated for their in vivo ANG II antagonistic activities. The in vivo activity was determined by the inhibition of the pressor response induced by infusion of ANG II in anaesthetized normotensive male rabbits. The in vivo experiments showed that compounds **11a** and **11c** did not significantly decrease mean arterial blood pressure, whereas **11b** with phenyl tetrazole moiety at the *m*-position showed moderate, however, comparatively better activity compared to the **11a** and **11c** (Fig. 4).

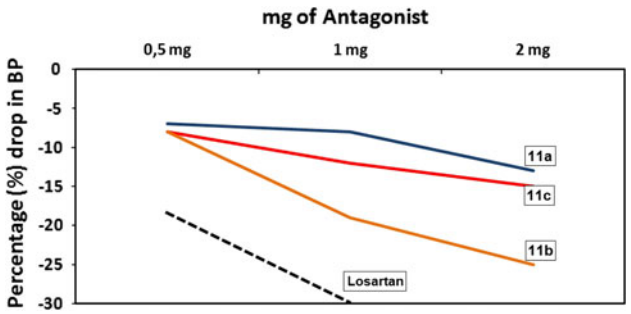

Fig. 4 Percentage (%) drop in mean blood pressure following three boluses of 0.5, 1 and 2 mg of each compound in anaesthetized rabbits made hypertensive by constant infusion of ANG II

Structure–activity relatioships

In vitro and in vivo results showed moderate, but higher activity of **11b**, rather than the *o*- and *p*-counterparts, in agreement with molecular modelling studies. These studies supported that the global minimum conformation of the **11b** analogue bearing the three pharmacophore groups, imidazole, phenyl and tetrazole distanced identically to the conformation of EXP3174, in contrast with **11a**, **11c**.

The conformations of the two rings (imidazole and phenyl) of the synthesized compounds and EXP3174 were tethered in several superimpositions (Fig. 5) in order to determine the orientation of the essential for receptor–substrate interaction tetrazole group, which is in evident spatial proximity between **11b** conformer and EXP3174. Ultimately, even though the tetrazole group seemed to be appropriately positioned, the shortening of the biphenyl group, the presence of an electron-withdrawing ester group and the lack of an aliphatic electron-donating group as in all Sartans essential for higher affinity and activity, could justify the moderate biological activity of **11b**. Consequently, the proper pharmacophore spacing is of primary importance in non-peptide antagonists for high binding affinity.

Moreover, the binding experiment results indicate a different orientation of the pharmacophores of the ligands. All docked poses for **11a–c** and EXP3174 were similar, with close RMSD values, indicating a stable ligand–receptor interaction model. EXP3174 also has the advantage of a more extended conformation, interacting with all the helices contributing amino acids to the binding site (Fig. 6). The main amino acids participating in hydrogen bond interactions were S3.33(109), L(191), N5.43(200) and Y7.43(292). Hydrophobic contacts stated the higher affinity of the *m*- against the *o*- and *p*-compounds. All conformers presented interactions with the critical residues of V3.32(108), L3.36(112), Y3.37(113), L(191), K5.42 (199), G5.46(203), F5.47(204), W6.48(253) and H6.51 (256) (Fig. 7).

Specifically, the best docked pose for each of the four compounds was further examined in order to give an elaborate visual explanation to the in vivo experiments.

EXP3174 fits in the binding site with the two phenyl rings interacting with the TM3 and TM5 residues and especially with K5.42(199) of the binding pocket. The imidazole group is in spatial proximity with the residues I7.39(288) Y7.43(292) of TM7 and the important tetrazole

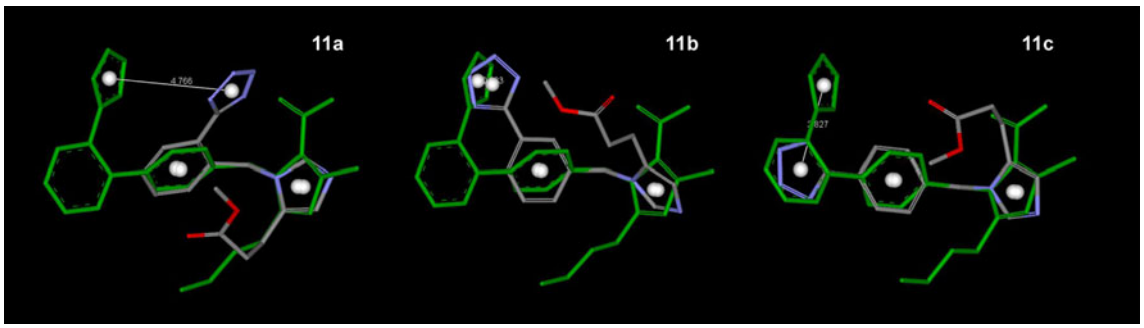

Fig. 5 Superimposition between EXP 3174 and **11a–c** compounds, respectively, illustrating spatial pharmacophore proximity

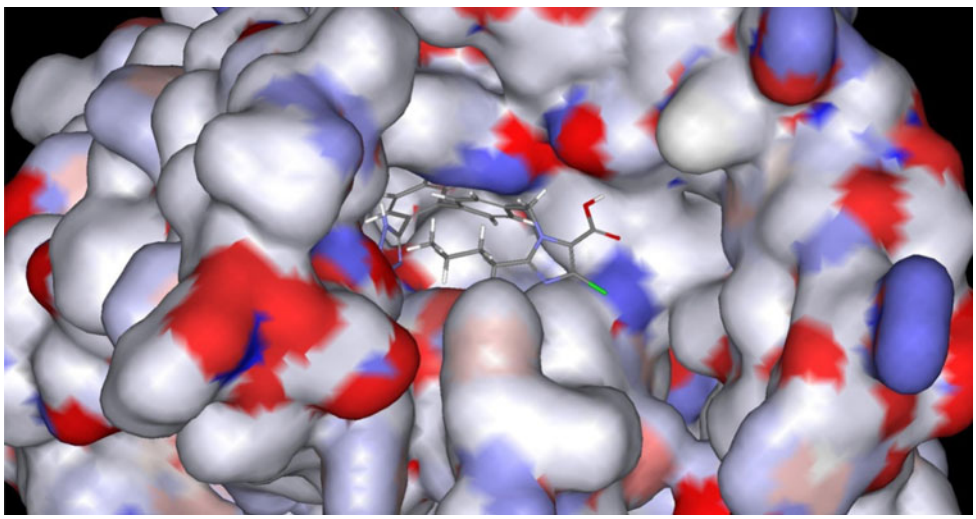

Fig. 6 Overview of EXP3174 in the binding site, formed between the TM3, TM5, TM6 and TM7 helices. The molecular surface is colour-coded by interpolated partial atom charge of nearest neighbours to the surface. The extracellular loops are not present for better visualization

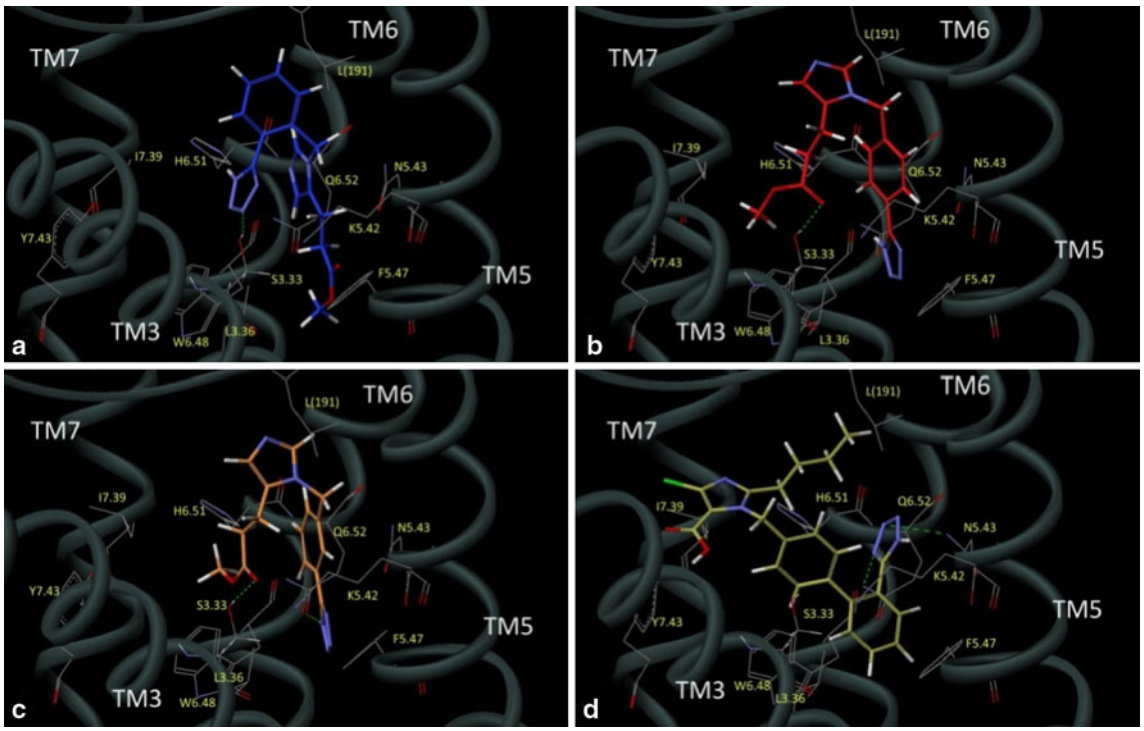

Fig. 7 Binding modes of the tested compounds, compared to EXP3174. Transmembrane helices 1, 2 and 4 are not visible for better clarity. Compounds **11a–c** (**a–c**) and EXP3174 (**d**) are presented

group in radius less than 3 Å, with N5.43(200) of TM5 and H6.51(256), Q6.52(257) of TM6. On the contrary, the **11a–c** poses with the highest affinity bind in a different manner, due to their smaller volume than EXP3174 of ~70% according to their van der Waals surface area (Fig. 7). **11a** has a totally different orientation than **11b** and **11c**, placing phenyl group far from the lipophilic pocket of the interaction site. Conformers **11b** and **11c** share a similar orientation but with one essential difference. Even though their phenyl and carbonyl groups interact with K5.42(199), N5.43(200) and S3.33(109), respectively (helices 3 and 5), their main contradiction is the *m*- conformer's methyl ester group which interacts with the side chain of W6.48(253). This proximity to the TM6 helix can interpret the increased affinity of **11b** to the AT1 receptor.

Conclusion

This study describes the synthesis and biological evaluation of a series of *o-, m-* and *p*-benzyl tetrazole derivatives **11a–c** as potential ANG II AT1 receptor antagonists, based on urocanic acid. The synthetic strategy of the target compounds **11a–c** included a facile few step method with high yields. Compound **11b** with tetrazole moiety at the *m*-position showed moderate, however, higher activity compared to the *o*- and *p*-compounds **11a** and **11c**, respectively. The *m*-substituted tetrazole in **11b** results in the accommodation of the imidazole and tetrazole groups towards TM3 and TM5 helices, as well as the proximity of the methyl ester group to W6.48(253) and TM6. Lower activity of **11b** compared to Losartan was due to (1) the lack of a lipophilic butyl pharmacophore group in the imidazole moiety necessary for binding in AT1 receptor antagonists (2) the smaller molecular weight and volume of our compounds than EXP3174, which eliminate their interaction with the important TM7 region of the binding site and (3) the shorter length of the phenyl template compared to the biphenyl moiety, necessary for high affinity to the receptor's lipophilic pocket, as well as proper spacing of pharmacophore groups and activity.

Acknowledgments This research project was supported by the Ministry of Development, General Secretariat of Research and Technology of Greece [EPAN: "IRAKLIS" YB 84 (B321/2005)]. We thank Dr Andreas Papapetropoulos for providing primary rat aortic smooth muscle cells (RASMC). Also, we would like to thank Dimitris Vahliotis (Instrumental Analysis Laboratory, University of Patras) for recording the NMR spectra.

References

Anthony NJ, Gomez RP, Schaber MD, Mosser SC, Hamilton KA, O'Neill T, Koblan KS, Graham SL, Hartman GD, Shah D, Rands

E, Kohl E, Gibbs JB, Oliff A (1999) Design and in vivo analysis of potent non-thiol inhibitors of farnesyl protein transferase. J Med Chem 42:3356–3368

Carini DJ, Duncia JV, Aldrich PE, Chiu AT, Johnson AL, Price WA, Santella JB, Wells J, Wexler R, Wang C, Yoo SE, Timmermans PBMWM (1991) Nonpeptide angiotensin II receptor antagonists: the discovery of a series of *N*-(biphenylmethyl)imidazoles as potent, orally active antihypertensives. J Med Chem 34:2525–2547

Cherezov V, Rosenbaum DM, Hanson MA, Rasmussen SG, Thian FS, Kobilka TS, Choi HJ, Kuhn P, Weis WI, Kobilka BK, Stevens RC (2007) High-resolution crystal structure of an engineered human beta2-adrenergic G protein-coupled receptor. Science 318:1258–1265

Chiu AT, McCall DE, Price WA, Wong PC, Carini DJ, Duncia JV, Wexler RR, Yoo S-E, Johnson AL, Timmermans PBMWM (1990) Angiotensin II receptor antagonists. VII. Cellular and biochemical pharmacology of DuP 753, an orally active antihypertensive. J Pharmacol Exp Ther 252:719–725

Clement M, Martin SS, Beaulieu ME, Chamberland C, Lavigne P, Leduc R, Guillemette G, Escher E (2005) Determining the environment of the ligand binding pocket of the human angiotensin II type I (hAT1) receptor using the methionine proximity assay. J Biol Chem 280:27121–27129

Duncia JV, Chiu AT, Carini DJ, Gregory GB, Johnson AL, Price WA, Wells GJ, Wong PC, Calabrese JC, Timmermans PBMWM (1990) The discovery of potent nonpeptide angiotensin II receptor antagonists: a new class of potent antihypertensives. J Med Chem 33:1312–1329

Dzau VJ (1994) Cell biology and genetics of angiotensin in cardiovascular disease. J Hypertens 12:421–429

Kubo K, Kohara Y, Yoshimura Y, Inada Y, Shibouta Y, Furukawa Y, Kato T, Nishikawa K, Naka T (1993) Nonpeptide angiotensin II receptor antagonists Synthesis and biological activity of benzimidazoles. J Med Chem 36:2343–2349

Lam S, Choy M (2007) Aliskiren: an oral renin inhibitor for the treatment of hypertension. Drug Highlight Cardiol Rev 15:316–323

Lauth-de Viguerie N, Sergueeva N, Damiot M, Mawlawi H, Riviere M, Lattes A (1994) Selective *N*-alkylation of *(E)*-urocanic acid. Heterocycles 37:1561–1578

Luitjen JG, Janssen MJ, Van Der Kerk G (1963) New organotin compounds containing a tin–nitrogen linkage. J Recl Trav Chim Pays Bas 81:202–205

Matsoukas J, Hondrelis J, Keramida M, Mavromoustakos T, Makriyannis A, Yamdagni R, Wu Q, Moore G (1994) Role of the NH2-terminal domain of angiotensin II (ANG II) and [Sar1]angiotensin II on conformation and activity. NMR evidence for aromatic ring clustering and peptide backbone folding compared with [des-1, 2, 3]angiotensin II. J Biol Chem 269:5303–5312

Matsoukas J, Agelis G, Wahhab A, Hondrelis J, Panagiotopoulos D, Yamdagni R, Wu Q, Mavromoustakos T, Maia H, Ganter R, Moore G (1995) Differences in backbone structure between angiotensin II agonists and type I antagonists. J Med Chem 38:4660–4669

Matsoukas J, Ancans J, Mavromoustakos T, Roumelioti P, Vlahakos DV, Yamdagni R, Wu Q, Moore G (2000) The design and synthesis of a potent angiotensin II cyclic analogue confirms the ring cluster receptor conformation of the hormone angiotensin II. J Bioorg Med Chem 8:4353–4360

Mirzadegan T, Benko G, Filipek S, Palczewski K (2003) Sequence analyses of G-protein-coupled receptors: similarities to rhodopsin. Biochem 42:2759–2767

Patny A, Desai PV, Avery MA (2006) Ligand-supported homology modeling of the human angiotensin II type 1 (AT1) receptor: insights into the molecular determinants of telmisartan binding. Proteins 65:824–842

Pirrung MC, Pei T (2000) Synthesis of (±)-homohistidine. J Org Chem 65:2229–2230

Sisido K, Nabika K, Isida T, Kozima S (1971) Formation of organotin-nitrogen bonds III, *N*-trialkyltin-5-substituted tetrazoles. J Organomet Chem 33:337–346

Thomas AP, Allot CP, Gibson KH SJ, Major JS, Masek BB, Oldham AA, Ratcliffe AH, Roberts DA, Russel ST, Thomason DA (1992) New nonpeptide angiotensin II receptor antagonists. 1. Synthesis, biological properties, and structure–activity relationships of 2-alkyl benzimidazole derivatives. J Med Chem 35:877–885

Tuccinardi T, Calderone V, Rapposelli S, Martinelli A (2006) Proposal of a new binding orientation for non-peptide AT1 antagonists: homology modeling, docking and three-dimensional quantitative structure–activity relationship analysis. J Med Chem 49:4305–4316

Turner R, Matsoukas J, Moore G (1990) Tyrosinate flyorescence life times for oxytocin and vasopressin in receptor simulating environments: relationship to biological activity and ^{1}H-NMR data. Biochem Biophys Res Commun 171:996–1001

Turner R, Matsoukas J, Moore G (1991) Fluorescence properties of angiotensin II analogues in receptor-simulating environments: relationship between tyrosinate fluorescence lifetime and biological activity. Biochim Biophys Acta 1065:21–28

Wong PC, Price WA Jr, Chiu AT, Duncia JV, Carini DJ, Wexler RR, Johnson AL, Timmermans PBMW (1990) Nonpeptide angiotensin II receptor antagonists. XI. Pharmacology of EXP 3174 an active metabolite of DuP 753, an orally active antihypertensive agent. J Pharmacol Ther 255:584–592

Wyvratt MJ, Patchett AA (1985) Recent developments in the design of angiotensin-converting enzyme inhibitors. Med Res Rev 5:485–531

Yanagisawa H, Amemiya Y, Kanazaki T, Shimoji Y, Fujimoto K, Kitahara Y, Sada T, Mizuno M, Ikeda M, Miyamoto S, Furukawa Y, Koike H (1996) Nonpeptide angiotensin II receptor antagonists: synthesis, biological activities, and structure–activity relationships of imidazole-5-carboxylic acids bearing alkyl, alkenyl, and hydroxyalkyl substituents at the 4-position and their related compounds. J Med Chem 39:323–338